ADVANCED ENGINEERING MATERIALS
www.aem-journal.com

# Accelerating Auxetic Metamaterial Design with Deep Learning

*Jackson K. Wilt, Charles Yang, and Grace X. Gu**

**Metamaterials can be designed to contain functional gradients with negative Poisson's ratio (NPR) that have counterintuitive behavior compared with monolithic materials. These NPR materials, referred to as auxetics, are relevant to engineering sciences because of their unique mechanical expansion. Previous studies have explored compliant actuators using analytical and numerically derived mechanics of materials principles. However, the control of compliant gradient mechanisms frequently uses complex analytical equations combined with traditional control algorithms, making them difficult to design. To confront the design processes and computational load, herein, machine learning is used to predict errors in compliant auxetic designs based on a mathematically optimal deformation. Finite element analysis and experimental specimens validate the theoretical mechanical behavior of a specific auxetic configuration as well as demonstrate the capabilities of additive manufacturing of graded auxetic materials. Pseudorandomized images and their respective computational deformation results are used to train a regressive model and predict the deviation from optimal behavior. The model predicts the deviation from the desired behavior with a mean average percent error below 5% for the validation set. Subsequently, a scalable workflow design process connecting the unique performance of auxetics to machine learning design predictions is proposed.**

Most monolithic engineering materials have positive Poisson's ratio and contract laterally relative to the direction of imparted strain. However, auxetics are a class of materials that expand laterally to the direction in which they are strained, exhibiting negative Poisson's ratio (NPR).[1,2] The key to an auxetic material's NPR is the internal structural mechanism that creates a rotational or leveraging effect of unit cell struts to the surrounding cells causing counterintuitive expansion.[3–5] Combining an array of auxetic cells forms metamaterials with tunable gradient properties depending on the unit cell geometry used and concentrations of the respective Poisson's ratio values.[6] Many unit cell architectures have been studied; however, significant focus has been conducted on the variations of the reentrant honeycomb cell which behaves within a range of strain, as an effective NPR unit cell expanding positively in all directions with positive imparted strain.[7–9] Reentrant honeycomb cells are the focus of this study because of their large basis of research and relative geometric simplicity for tuning behavior.[10] Due to the unique mechanical properties of auxetics, NPR materials are used in engineering applications, especially when the materials undergo significant deformation.[11] However, the behavior of auxetics in soft-bodied materials is still being developed and makes their interaction in applications difficult to predict.

Applications of auxetic metamaterials have been explored in previous literature, ranging from impact lattice structures, medical stents, and others described in depth in previous review studies, whose main function is derived from their behavior under strain.[12,13] Of particular importance to our work is the application of auxetic metamaterials in 2D and 3D soft bodies due to this counterintuitive deformation behavior.[14] 2D elastomeric lattices are currently in use and being explored in sportswear and biomedical films that are able to conform to the body. However, out-of-plane strain is still a design fault, impeding progress for both applications.[15] 3D application studies have also been conducted on the use of biomimetic soft-body manipulators using fluidic control. Manipulator applications utilize conventional kinematic models for simple movements but such models restrain researchers to a predefined control methodology when creating more complex control systems.[16] Researchers have explored auxetic geometries to create a soft-bodied cylinder using auxetic cell buckling failure for angular actuation.[17] This work demonstrated fundamental aspects of NPR in 3D actuation and incentivized our study to develop a workflow for designing dynamic auxetics, using a similar form of an angularly actuated cylinder. Aside from the pressure-driven actuation control system, in many of these cases, the only way for the intricate structures to be manufactured is through detailed casting or, as we use in our approach, via an additive manufacturing system. Additive manufacturing is an ideal method of creating various types of metamaterials because 3D printers are capable of fabricating complex architectures.[18–24] The coupled ability to rapidly and iteratively discover new designs with machine learning and experimentally validate results with additive manufacturing marks a novel discovery process in manufacturing and materials characterization.[25,26] The programmability of the additive

J. K. Wilt, C. Yang, Prof. G. X. Gu
Department of Mechanical Engineering
University of California, Berkeley
6177 Etcheverry Hall, Berkeley, CA 94720-1740, USA
E-mail: ggu@berkeley.edu

The ORCID identification number(s) for the author(s) of this article can be found under https://doi.org/10.1002/adem.201901266.

**DOI: 10.1002/adem.201901266**

 

process is exploited through the digital placement of the cells during the design of the metamaterials and when outputting the printer's manufacturing paths.

The behavior of auxetic metamaterials is derived from the geometrical intuition of deformation from constitutive material principles. Researchers from previous studies manually input the geometry of the unit cells to produce the desired Poisson's ratio, which is usually time consuming when designing for specific applications.[27] Some studies use computer-aided modeling programs to approach auxetic designs with conventional topology optimization tools, which require intermittent computational analysis confirming feasibility.[28] These preliminary studies have accelerated the design of the metamaterial unit cells and their predicted behavior but are eventually impeded by complex analytical and numerical control models at larger scales. Relevant literature is just now addressing the limitations of conventional control systems and the application of machine learning to help establish their data acquisition systems and baseline control of soft manipulators.[29,30] Few studies have been conducted on the use of machine learning to enhance the design time of engineering metamaterials for actuating applications.

The flux of data generated by computational sciences has enabled the rise of machine learning for discovering patterns in scientific data. The advent of powerful open-source machine learning libraries, such as scikit-learn[31] and TensorFlow,[32] allows for trends to be gleaned from large-scale datasets for physical engineering applications. Previously, data-driven methodologies have been applied to crack propagation prediction models, in situ materials processing corrections, and composite material property prediction.[33–38] A convolutional neural network (CNN) is a specific machine learning model commonly used in computer vision applications. CNNs utilize the convolution operation to downsample multidimensional tensors, the weights and biases of which are updated according to stochastic gradient descent.[39] Recently, CNNs have been shown to be capable of predicting mechanical properties from 2D designs using CNN image regression.[40] In our case, the ability to predict nontrivial deformation solutions of materials with a geometric substructure is becoming increasingly important for the control systems of soft robotics and deployable structures. Hyperelastic material models have been studied for determining elastomer behavior, and it has been shown that by integrating geometrical substructures, empirical models output unconventional deformations.[41,42] Consequently, machine learning is used in this study to determine practical designs in a attempt to bypass potentially complex hyperelastic analytical methods.

The methodology behind this work is based on the use of finite element analysis (FEA) computational results to be used as machine learning labels for determining novel engineering designs of graded auxetics. The reentrant honeycomb cells only require the strut angle to be modified for evaluating the representative auxetic quality and provide simple metrics to be used in machine learning feature selection. We aim to supplement design time through machine learning and image processing as well as predicting metamaterial behavior from an engineered design. In addition, the study provides an avenue for nonexperts to interpret designs that could be useful for compliant manipulator designs. The experimental 2D and 3D specimens that are produced validate the theoretical mechanical behavior of a specific auxetic configuration which aids in setting the optimal reference function for the FEA. Using a CNN, a regression model is created for calculating the difference between the desired deformation behavior and actual deformation. The resulting data-driven model is proposed as a scalable machine learning workflow.

Initially, 2D Python FEA and meshing suites are used to simulate a high-throughput array of auxetic metamaterial lattices for uniaxial stress studies. Using FEA and meshing allows us to quickly iterate over design choices and make the eventual data science analysis with efficiently calculated simulations. Here the process is summarized into the choice of the unit cell, construction of the mesh, analysis of the mesh, and graphical results.

The reentrant honeycomb unit cell is used because of its relatively simple geometry for setting auxetic quality in individual unit cells where the variation of Poisson's ratio attainable is shown in **Figure 1**a. Parameters for the auxetic quality are determined by the length and angle of the unit cell's trusses. Two dimensionally, the material cross section is greater in the purely auxetic cell as compared with the nonauxetic cell by 22.6% because the trusses are kept at the same width but form a larger surface area in the auxetic cell. This surface area imbalance is dominated by the auxetic or nonauxetic geometry and is not envisioned to impact the theoretical Poisson's ratio which is based on the angles of the trusses.

The Python library Pygmsh then assigns object identifiers to the nodes and placement in a computational field with the maximum metamaterial dimensions of $11 \times 11$. This size is chosen because it is approximately the size of the metamaterial lattices from other studies and large enough to demonstrate regionally significant metamaterial deformation. Each unit cell in the meshing module is simulated as a $2\,\text{cm} \times 2\,\text{cm}$ geometrical cell where the set Poisson's ratio determines the angle of the truss. The cells and their assigned Poisson's ratio values establish an array from the convention in Figure 1a, where the angle of the top-right truss relative to the horizontal $x$-axis determines the magnitude and sign of Poisson's ratio for each cell. The mesh generation propagates nodes based on the refinement specified within the Python code. The level of refinement is chosen where the resulting Jacobian is viable and where the simulation can reach convergence on the order of several minutes.

After the nodes are propagated, the SolidsPy physics module creates a computational graph from the nodes to impart uniaxial stress onto the top of the metamaterial. All simulations have a positive distributed force of $1000\,\text{N m}^{-1}$ on the top beam of the material and fixed on the bottom, using properties for NinjaFlex thermoplastic polyurethane (TPU), $E = 0.1124$ GPa and $\nu = 0.344$. Although we use an elastomer in the simulations, we operate on a linear elastic model because the strain of a bulk material would retain a relatively uniform Young's modulus at a longitudinal strain of approximately $\varepsilon_y = 0.3$ for all simulations.

Figure 1b,c compares auxetic distributions from the regional auxetic placement function within the meshing code as well as their final deformation states. The resulting data are stored as $x$-displacement and $y$-displacement arrays for future data processing on the regional deformation of 2D metamaterials.

 

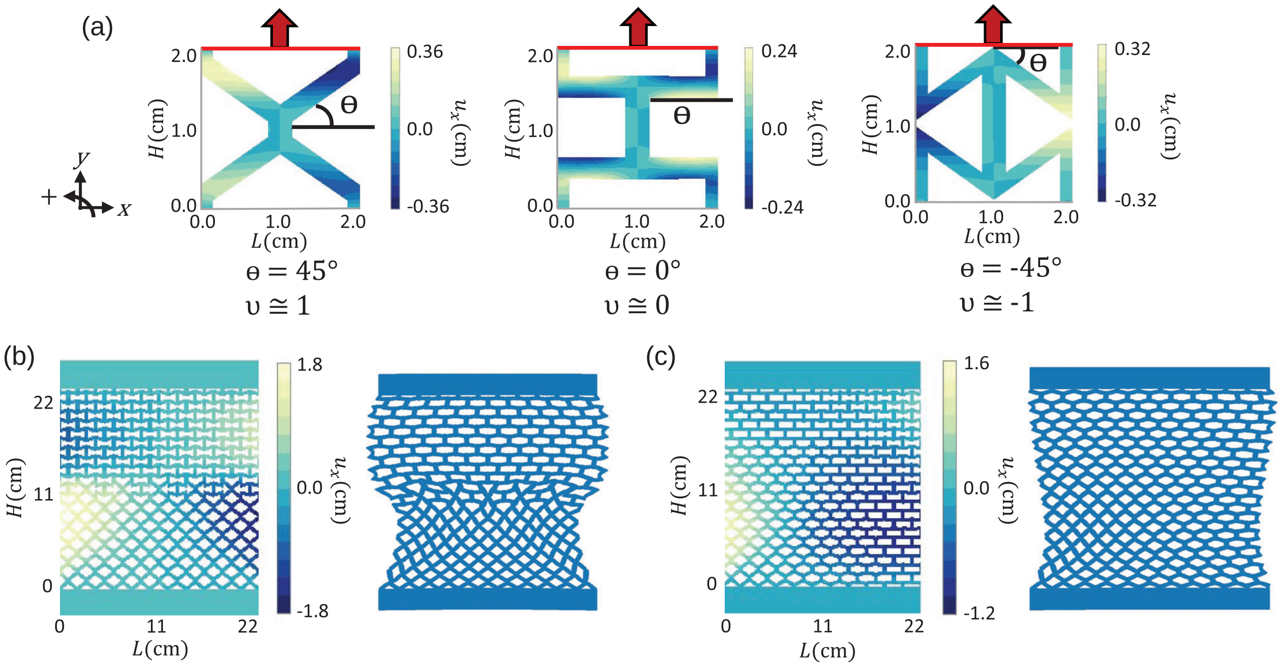


**Figure 1.** a) Individual unit cell H × L, *x*-axis deformation $u_x$, patterns by variation of angles $\theta$, and theoretical Poisson's ratio $\nu$, under 1/11th of full metamaterial loading. Two FEA metamaterial distributions under full 1000 N $m^{-1}$ loading, b) lower half nonauxetic upper half auxetic and c) gradient of nonauxetic bottom left to auxetic top right.

The 2D lattices are useful for visualizing the regional displacement effect, but a 3D manipulator design is an ideal outcome from the study because of the medical field's interest in soft actuators. An engineered function is created which will be referred to throughout the study as the optimal design or function because of its correlation with a potential medical actuator application. The optimal design defined in more geometrical and mechanical terms is selected to exhibit high theoretical expansion in the middle portion of the lattice by placing purely auxetic cells in the mid-section of the metamaterial with purely nonauxetic cells on the quarters above and below the middle portion. This optimal design is based on fundamentals for the mechanics of materials where the lattice expands laterally to the direction of stress based on concentrations of NPR in the material. To express the viability of the optimal design, a small panel of experimental testing is conducted to compare to the simulated model. NinjaFlex TPU is used as the engineering material for this study due to its low elastic modulus, relative to other printable thermoplastics, and the ability to reach the desired strain $\varepsilon_y = 0.3$ without plastic deformation. **Figure 2**a shows the graphical distribution of auxetic quality for the optimal 2D lattice and Figure 2b shows its empirical expansion under $\varepsilon_y = 0.3$. The optimal function is created in 2D which is capable of being wrapped around a cylindrical pressure vessel. Experimentation is conducted using a cylindrical tube with the auxetic lattice extruded on the cylinder's surface. A shell function in SolidWorks is applied to the cylinder to form small bellows out of the cellular geometry for pneumatic expansion. In Figure 2c, a graphic of deformation is shown, demonstrating the hoop and axial stress based on the mechanics of materials principles for pressure vessels. The expansion of the auxetic cells compared with the nonauxetic cells will theoretically cause greater NPR deformation and in turn cause the cylindrical sample to actuate angularly in the direction opposite the auxetic surfaces. The deformation process is shown from 0-psi in Figure 2d to a maximum pressure of 100-psi ($6.89 \times 10^5$ Pascals) in Figure 2e. The 100-psi maximum pressure extends the cylinder vertically in the *y*-direction by 3 cm measured from the center of the cap at 0-psi and angular tilt of the cylinder top $+10°$ from the reference *y*-axis in Figure 2. Greater angular displacement could be possible by increasing the depth of extrusion on the auxetic surface but would require more advanced additive printing systems that include support structures or with multimaterial printing using materials with different Young's moduli. These empirical tests confirm the theoretical basis for computational deformation of the 2D gradient auxetic FEA modules.

Building on the programmability of FEA, images are used instantiate the auxetic unit cell arrangement in the lattice. The image in **Figure 3**a shows the optimal function's auxetic distribution in the top portion of the material with a binary $\nu = -1$ and $\nu = 1$ Poisson's ratio value; the deformation concentration result is shown in Figure 3b. The machine learning aspect of iterating on random variations to predict displacement is inspired by architected materials found in nature and their evolutionary iterative design process. Mathematica is used to generate pseudorandom images using several image processing functions that create asymmetrical Rorschach (ink blot) images. The meshing program assigns the unit cell matrix values according to the image that Mathematica generates. Mathematica's pseudorandomized images are blurred using a Gaussian filter and applied to the $11 \times 11$ grid-creating images similar to Figure 3c. This image differs from the optimal image by containing theta angles as a

 

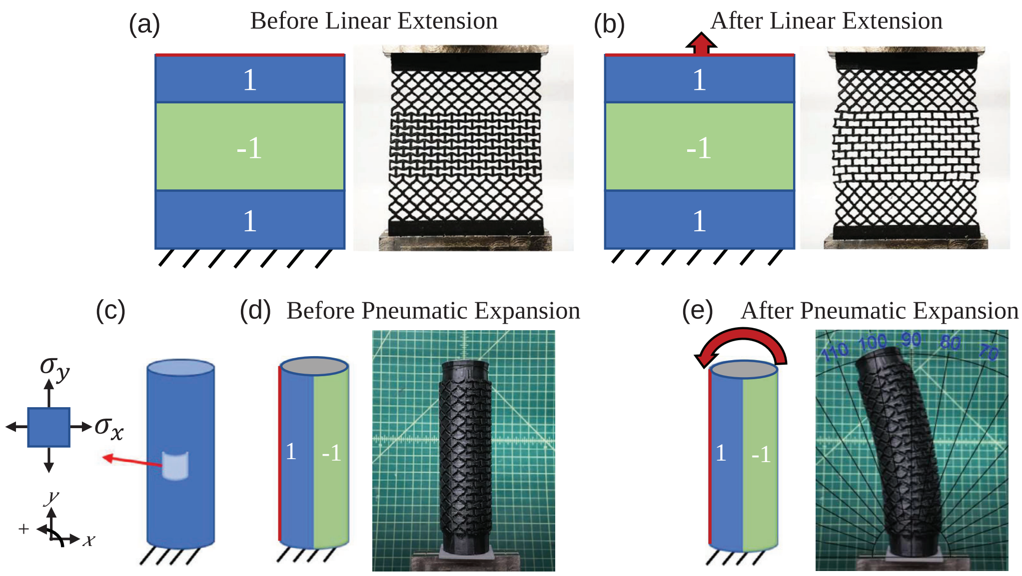


**Figure 2.** a) Optimally engineered lattice for angular displacement where $\nu = 1$ represents nonauxetic positive Poisson's ratio and $\nu = -1$ is auxetic NPR. b) Engineered lattice after extension. c) Fundamentals of pressure vessels expressed in a diagram using the 2D optimal lattice wrapped around a hollow cylinder. d) Cylinder print without pressure actuation. e) After pneumatic expansion of the cylinder.

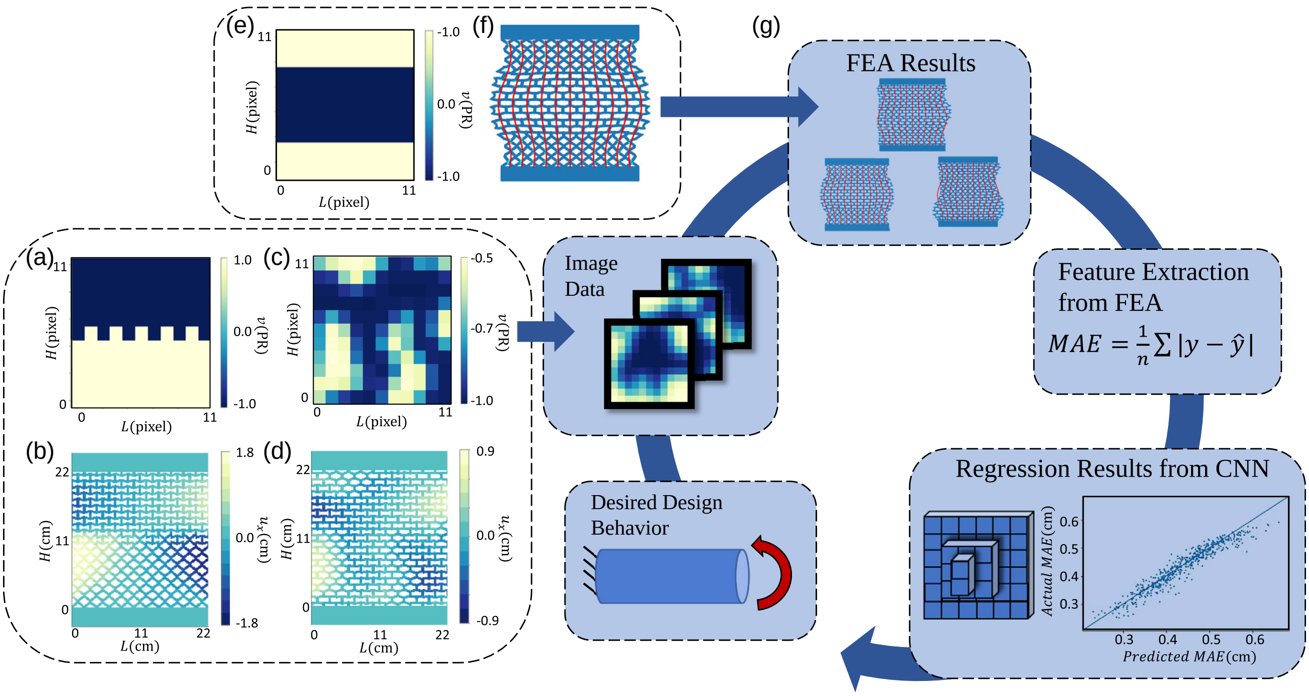


**Figure 3.** a) Pixelated image of half auxetic and half nonauxetic material H × L, 22 pixels × 22 pixels, and its b) resulting *x*-displacement graphs with dimensions H × L, 22 cm × 22 cm. c) Randomized material image with pixel dimensions of H × L, 22 pixels × 22 pixels, and its d) resulting *x*-displacement graphs with dimensions H × L, 22 cm × 22 cm. e) Optimal design along with f) the mathematical correlation with its behavior in red lines. g) Machine learning workflow model demonstrating the design cycle of the auxetic material.

distributed gradient of auxetic values within the range from $\nu = -1$ to $\nu = 1$ values of Poisson's ratio and is shown with its corresponding deformation in Figure 3d. The range of images generated is then used to set the auxetic value of a 11 × 11 image, imparting the auxetic quality to the individual unit cells for FEA simulation. The FEA solver then performs the simulation based on material properties for NinjaFlex TPU and outputs the uniaxial stressed state of deformation for the input image. The optimal input design in Figure 3e is chosen because of its intuitively monomodal expansion for the metamaterial from the high concentration of auxetic cells in the middle half of the material and the nonauxetic cells in the quarters above and below the middle. In Equation (1), we iterate through the free parameters $A$, $h$, $b$, and $k$ to be the closest numerical approximation to the simulated theoretically optimal deformation. Figure 3f shows a deformed auxetic lattice of the optimal design with the waveform function in Equation (1) using calculated variables $A$, $h$, $b$, and $k$ to graph the 11 red lines coinciding with the unit cell centers. The function in Equation (1) is compared with the randomized $x$-displacements for each unit cell to calculate mean absolute error (MAE). The machine learning model uses the calculated MAE, as described by Equation (2) between the optimal design $x$-displacement, $\hat{y}$, and randomized design $x$-displacement results, $y$, as the machine learning labels. Only $x$-displacement arrays are used in training the machine learning model to study the capabilities of a basic one-output model in a system that otherwise could perform as a more complex multioutput model. The resulting MAE labels of the machine learning model are paired with the respective $11 \times 11$ randomized image for creating sample sets. Figure 3g shows the machine learning workflow for CNN as well as the complete design iteration process for a data-driven control model. Using TensorFlow with a Keras deep learning backend, a regressive neural network is formed using a 16-layer filter size with four convolutions and one fully stacked dense layer. After completing the training of the machine learning model on 4500 pseudorandomized images, we predict the auxetic architecture's capability to adhere to the mid-section of NPR deformation function. The cross-validation set consists of 500 samples.

$$\hat{y} = A \sin\left(\frac{(x-h)}{b}\right) + k \tag{1}$$

$$\mathrm{MAE} = \frac{1}{n}\sum |y - \hat{y}| \tag{2}$$

After exploring the design space, the diversity of auxetic quality causes an array of design choices that behave within a range of error to the optimal function value. The primary application achieved in the study is the prediction of expansion behavior with regression using distributed auxetic and nonauxetic unit cells. The regression estimation values chart in **Figure 4**a produces an $R^2$ value of 0.91, which suggests convergence and implies that a higher accuracy can be achieved with more high-quality training samples. The results displayed in the MAE histogram from Figure 4b are used to calculate the values for the mean squared error of 0.00057, which demonstrates a relatively low error value in machine learning validation. The trained model for this study predicts the deviation of the expansion behavior relative to the optimal design with a mean average percent error of 4.2%. The trained model predicts a potential design image using samples from the validation set in Figure 4c and its solution in Figure 4e with the actual value of 0.23 cm MAE and a predicted value of 0.27 cm (percent error = 17.39%). Alternatively, an undesirable design image is predicted in Figure 4d where its deformation in Figure 4f shows the sample measured at 0.66 cm MAE and predicted at 0.60 cm (percent error = 9.09%). These predictions are at a higher mean average percent error margin than that of the moderate error cases because the model is trained on a larger number of random albeit evenly distributed auxetic quality samples. In the future, applying a suite of mathematical functions for generating training images instead of the pseudorandomized approach is likely to aid in determining favorable engineering design images. These results show that a basic machine learning model with a single-feature image input and single-value output can be expanded in the future using different configurations of unit cells, optimized design functions, 2D metamaterial shapes, and feature selection. We also plan to use more advanced FEA models by setting the elastic modulus of the simulated material to be a function of strain according to the respective material used and degree of strain.

Using previously deformed metamaterial data with the implementation of a new mathematical function expedites the design time of auxetic distribution in a material for a specified design behavior. This machine learning method offers design combinations that are not intuitive compared with the theoretically optimum configuration. Previous literature focuses on traditional topology optimization and advanced mechanics to guide design; however, this study reveals some aspects of feature selection using computational data streams to design for 2D and consequently, 3D deformation. Using the prediction from the machine learning model, a design was selected at a low predicted MAE value relative to the function and displayed a design representative of the intended expansion. Another important aspect of this study is drawing on the core principles of engineering and the practicality of using common commercial materials and open-source repositories. Designing a material with specific deformation characteristics requires design time, mechanics of materials expertise, and iterative techniques with traditional topology optimization. A researcher may only need to specify the formulaic behavior of the material for this machine learning portion to develop favorable arrangements, in essence, programming material deformation. At scale, this approach is not intended to displace analytically derived solutions but supplement design time in complex engineering applications and possible design combinations in soft-bodied actuation. The soft robotics implications of this study confirm a pneumatic approach for the axial and angular displacement of a soft-body structure with an auxetic skin. Deformable soft-body entities can be used in biomedical and human interactive technologies with more comprehensive studies of high-performance architected elastomers. The goal for future applications entails testing 3D deployable geometries and robotic gripping tools, using both auxetics as the mechanisms for differential expansion and machine learning for their control systems or design selection.

## Experimental Section

Programming the meshing software consisted of two primary open-source Python packages Pygmsh[43] and SolidsPy.[44] Pygmsh generated a finely meshed surface for an accurate physical representation. SolidsPy was used as the FEA tool to determine the deformation and strain of the structure by imparting a force on the top beam as well as constraining it to move in the $y$-direction and fixing the bottom beam. The array created a 22 cm 22 cm metamaterial lattice in the computational space with an average truss width of 0.025 and 3 cm solid support beams on the top and bottom of the sample. The Python packages are continually being updated and, in the future, will likely be more resilient to complex geometries for testing parameters. We created a Mathematica script to

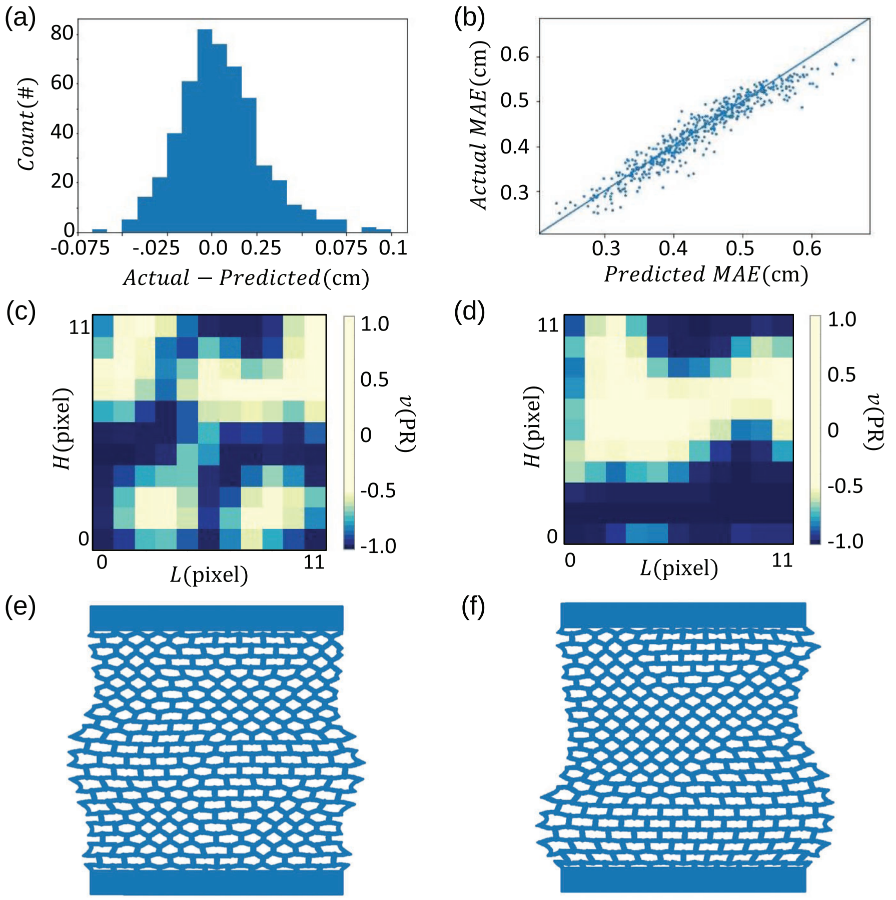


**Figure 4.** a) MAE diagram and b) actual versus predicted values regression. c) Image of possible unique predicted solution architecture and d) image of the highest predicted error (right side). e) Deformation of random potential solution and f) deformation of high error image.

generate the images with built-in random radial functions. A Python application programming interface-accessed Mathematica toolkits and algorithms to produce a set of semirandomized images using radial tracing were generated and then resized using OpenCV. The fused deposition modeling printer used for the empirical samples was a Prusa i3 MK3. The rectangular prism of the 2D sample was additively manufactured with dimensions $11\,\text{cm} \times 14\,\text{cm} \times 0.25\,\text{cm}$, an average truss width of 0.0125, and 1.5 cm solid beams on the top and bottom. Empirical testing was one-half of the dimensionality of the 2D computational design to fit the testing apparatus. The dimensions of the cylindrical prism were 3 cm diameter × 14 cm height and the bellows extruded 0.3 cm from the surface with a wall thickness of 0.08 cm. The tensile testing system used was a Tenson Universal Testing Machine at a vertical strain of $\varepsilon_y = 0.3$ for the experimental samples. A Gaussian filter was applied to the asymmetrical Rorschach image generation function from Mathematica. This was to create a more gradual transition from a purely auxetic cell to a non-auxetic cell. The equation for this blurring is given below, Equation (3), with $\sigma = 10$.

$$G(x, y) = \frac{1}{2\pi\sigma^2} e^{-(x^2+y^2)/(2\sigma^2)} \tag{3}$$

## Acknowledgements

The authors acknowledge support from the Extreme Science and Engineering Discovery Environment (XSEDE) by National Science Foundation, grant number ACI-1548562. In addition, the authors acknowledge support from NVIDIA GPU Seed Grant, Johnson & Johnson WiSTEM2D Scholars Award, and Amazon Research Award.

## Conflict of Interest

The authors declare no conflict of interest.

## Keywords

additive manufacturing, auxetic materials, machine learning, metamaterials

Received: October 21, 2019
Revised: December 10, 2019
Published online:

[1] Y. Prawoto, *Comput. Mater. Sci.* **2012**, *58*, 140.
[2] X. Ren, R. Das, P. Tran, T. D. Ngo, Y. M. Xie, *Smart Mater. Struct.* **2018**, *27*, 023001.
[3] T.-C. Lim, *Phys. Stat. Sol. RRL* **2017**, *11*, 1600440.
[4] Y. Jiang, Y. Li, *Adv. Eng. Mater.* **2017**, *19*, 1600609.

[5] Y. Jiang, Y. Li, *Adv. Eng. Mater.* **2018**, *20*, 1700744.
[6] Q.-T. Deng, Z.-C. Yang, *Mater. Express* **2016**, *6*, 461.
[7] D. Rayneau-Kirkhope, *Sci. Rep.* **2018**, *8*, 12437.
[8] T. Li, Y. Chen, X. Hu, Y. Li, L. Wang, *Mater. Des.* **2018**, *142*, 247.
[9] C. Yang, H. D. Vora, Y. Chang, *Smart Mater. Struct.* **2018**, *27*, 025012.
[10] K. K. Saxena, R. Das, E. P. Calius, *Adv. Eng. Mater.* **2016**, *18*, 1847.
[11] M. Mir, M. N. Ali, J. Sami, U. Ansari, *Adv. Mater. Sci. Eng.* **2014**, *2014*, 1.
[12] X. L. Ruan, J. J. Li, X. K. Song, H. J. Zhou, W. X. Yuan, W. W. Wu, R. Xia, *Int. J. Appl. Mech.* **2019**, *10*, 1850105.
[13] S. K. Bhullar, A. T. Mawanane Hewage, A. Alderson, K. Alderson, B. G. Martin, *Adv. Mater.* **2013**, *2*, 42.
[14] S. Janbaz, F. S. L. Bobbert, M. J. Mirzaali, A. A. Zadpoor, *Mater. Horiz.* **2019**, *6*, 1138.
[15] K. I. Jang, H. U. Chung, S. Xu, C. H. Lee, H. Luan, J. Jeong, H. Cheng, G. T. Kim, S. Y. Han, J. W. Lee, J. Kim, M. Cho, F. Miao, Y. Yang, H. N. Jung, M. Flavin, H. Liu, G. W. Kong, K. J. Yu, S. I. Rhee, J. Chung, B. Kim, J. W. Kwak, M. H. Yun, J. Y. Kim, Y. M. Song, U. Paik, Y. Zhang, Y. Huang, J. A. Rogers, *Nat. Commun.* **2015**, *6*, 6566.
[16] D. Rus, M. T. Tolley, *Nature* **2015**, *521*, 467.
[17] A. Lazarus, P. M. Reis, *Adv. Eng. Mater.* **2015**, *17*, 815.
[18] M. J. Mirzaali, A. Caracciolo, H. Pahlavani, S. Janbaz, L. Vergani, A. A. Zadpoor, *Appl. Phys. Lett.* **2018**, *113*, 241903.
[19] M. Wagner, T. Chen, K. Shea, *3D Print. Addit. Manuf.* **2017**, *4*, 133.
[20] J. R. Raney, J. A. Lewis, *MRS Bull.* **2015**, *40*, 943.
[21] Z. Vangelatos, G. X. Gu, C. P. Grigoropoulos, *Extreme Mech. Lett.* **2019**, *33*, 100580.
[22] G. X. Gu, F. Libonati, S. D. Wettermark, M. J. Buehler, *J. Mech. Behav. Biomed. Mater.* **2017**, *76*, 135.
[23] G. X. Gu, M. Takaffoli, M. J. Buehler, *Adv. Mater.* **2017**, *29*, 1700060.
[24] J. Yeo, G. S. Jung, F. J. Martín-Martínez, S. Ling, G. X. Gu, Z. Qin, M. J. Buehler, *Phys. Script.* **2018**, *93*, 053003.
[25] C.-T. Chen, G. X. Gu, *MRS Commun.* **2019**, *9*, 556.
[26] G. X. Gu, C.-T. Chen, D. J. Richmond, M. J. Buehler, *Mater. Horiz.* **2018**, *5*, 939.
[27] D. Chen, X. Zheng, *Sci. Rep.* **2018**, *8*, 9139.
[28] J. Schwerdtfeger, F. Wein, G. Leugering, R. F. Singer, C. Korner, M. Stingl, F. Schury, *Adv. Mater.* **2011**, *23*, 2650.
[29] K. Nakajima, H. Hauser, T. Li, R. Pfeifer, *Soft Robot.* **2018**, *5*, 339.
[30] S. Bhagat, H. Banerjee, Z. Ho Tse, H. Ren, *Robotics* **2019**, *8*, 4.
[31] F. Pedregosa, G. Varoquaux, A. Gramfort, V. Michel, B. Thirion, *J. Mach. Learn. Res. 12*, 2825.
[32] M. Abadi, A. Agarwal, P. Barham, E. Brevdo, Z. Chen, G. S. C. C. Citro, A. Davis, J. Dean, M. Devin, S. Ghemawat, I. Goodfellow, A. Harp, G. Irving, M. Isard, Y. Jia, R. Jozefowicz, L. Kaiser, M. Kudlur, J. Levenberg, D. Mane, R. Monga, S. Moore, D. Murray, C. Olah, M. Schuster, J. Shlens, B. Steiner, I. Sutskever, K. Talwar, P. Tucker, V. Vanhoucke, V. Vasudevan, F. Viegas, O. Vinyals, P. Warden, M. Wattenberg, M. Wicke, Y. Yu, X. Zheng, *ArXiv* **2015**, arXiv:1603.04467v2.
[33] A. Rovinelli, M. D. Sangid, H. Proudhon, W. Ludwig, *NPJ Comput. Mater.* **2018**, *4*, 35.
[34] A. Rovinelli, M. D. Sangid, H. Proudhon, Y. Guilhem, R. A. Lebensohn, W. Ludwig, *J. Mech. Phys. Solids* **2018**, *115*, 208.
[35] W. Ma, F. Cheng, Y. Liu, *ACS Nano* **2018**, *12*, 6326.
[36] C. T. Chen, G. X. Gu, *Adv. Theory Simulat.* **2019**, *2*, 1900056.
[37] G. X. Gu, C.-T. Chen, M. J. Buehler, *Extreme Mech. Lett.* **2018**, *18*, 19.
[38] Z. Jin, Z. Zhang, G. X. Gu, *Manufact. Lett.* **2019**, *22*, 11.
[39] K. O'Shea, R. Nash, *ArXiv* **2015**, arXiv:1511.08458v2.
[40] C. Yang, Y. Kim, S. Ryu, G. X. Gu, *MRS Commun.* **2019**, *9*, 609.
[41] L. Chen, C. Yang, H. Wang, D. T. Branson, J. S. Dai, R. Kang, *Mech. Mach. Theory* **2018**, *130*, 109.
[42] H. Yang, G. Ganzosch, I. Giorgio, B. E. Abali, *Z. Angew. Math. Phys.* **2018**, *69*, 104.
[43] C. Geuzaine, J.-F. Remacle, *Int. J. Numer. Methods Eng.* **2009**, *79*, 1309.
[44] J. Gómez, N. Guarín-Zapata, *Parameters* **2018**, *50*, 2.0.